Ambient noise levels in north central Italy

S. Marzorati and D. Bindi

Istituto Nazionale di Geofisica e Vulcanologia, Via Bassini 15, I-20133, Milano, Italy (marzorati@mi.ingv.it)

[1] The characteristics of background seismic noise in north central Italy have been investigated by means of velocity power spectral analysis within the frequency range 0.1–15 Hz. The method proposed by McNamara and Buland (2004) has been applied to estimate the probability density function (PDF) of power spectra computed for ten different stations. Since the target region is the most industrialized area of Italy, a large variability among the power spectra for different sites is observed in the frequency range 1–15 Hz, with the noise levels at two stations exceeding the New High Noise Model (NHNM) of Peterson (1993). The 95th percentile of the PDF varies from −165 to −125 dB (relative to (m/s)^2/Hz). This variability could significantly affect the detection capabilities of a network installed for recording the small to moderate size seismicity occurring in north central Italy. We also observed that the dispersion of the powers, estimated at each site as the difference between the 95th and the 5th percentiles, shows a positive trend with frequency that can be ascribed to the diurnal variation of the background noise levels. In the frequency range 0.1–1 Hz, the dominant feature is the double frequency (DF) peak of microseisms generated by oceanic storms. At one of the considered stations, the seasonal variability of the maximum amplitude of the DF peak has been observed in the period from April 2004 to December 2005. Considering the barometric maps provided by the UK Meteorological Office, we observed that the strongest powers in the range 0.10–0.25 Hz occur when intense storms are present over the North Atlantic Ocean, whereas the measurements of the height, frequency, and azimuth of the sea waves at two buoys of the Rete Ondametrica Italiana deployed in the Adriatic and Tyrrhenian seas suggest that the DF microseisms in the frequency range 0.25–0.50 Hz are generated by storms over the Mediterranean Sea. Finally, the analyzed region is characterized by two large-scale geologic features, namely, the Po Plain and the Alps. The impedance contrast between these two units causes a noise reduction of about 10 dB in the frequency range 0.2–0.6 Hz.

1. Introduction

[2] The installation of a seismic network requires the selection of sites suitable for housing the recording stations. The site selection procedure is generally a sequence of compromises between the selected network geometry, which depends on the assumed monitoring purposes, and the criteria

that a given site has to meet for being suitable to house a station. The selection criteria are generally based on off-site and in-field studies [*Trnkoczy et al.*, 2002]. The off-site studies include several considerations that exploit the a priori knowledge of the geographic region of interest, such as consideration of the seismo-geological and topographic conditions, accessibility of the sites, data transmission and power considerations. Moreover, the presence of potential seismic sources acting in the analyzed region has also to be investigated during these studies. The off-site studies are followed by fieldwork at each potential site. During the visit at each site, the conclusions drawn from the off-site studies are checked (e.g., the easy of accessibility is verified, the availability of the power line is checked) and noise measurements are performed. The characterization of the noise range at a given site, as well as its spectral content, is an important task for establishing the theoretical performance of the seismic network. Since the characteristics of seismic noise depend greatly on both weather conditions and man-made activities, the noise windows should be acquired with a daily frequency and over periods long enough to sample all the features of the seismic noise variability. Moreover, the length of each acquired time window should allow to resolve the spectral noise characteristics in the frequency range typical of the sensor that has to be installed. A detailed description of site selection and the nature of seismic noise can be found in the IASPEI New Manual of Seismic Observatory Practice [*Bormann*, 2002; *Trnkoczy et al.*, 2002].

[3] In this work, we exploit noise measurements previously performed in several locations of north central Italy, to investigate the noise range for sites belonging to different geological settings, such as the alpine or large alluvial basin environments, and placed in areas with a different degree of urbanization. After a careful data processing, we apply a statistical approach based on power spectral density functions (PSDs) to evaluate and compare the range of seismic noise for different stations [*McNamara and Buland*, 2004]. We compare the characteristics of the background noise power with the level of anthropic noise and consider the weather conditions in the North Atlantic Ocean and in the Mediterranean Sea. Finally, the reduction of noise power in the microseism frequency band due to the seismic

impedance contrast between the Po Plain and the Alps is investigated.

2. Data Processing and Method

[4] Since we analyze data coming from several experiments not all designed for site selection purposes, the data set we handle is inhomogeneous in many aspects, such as data acquired by either short-period or broadband sensors, different settings of the acquisition protocols, and different extension in time of the monitoring activity at each site. We investigate the variation of seismic noise by computing the Probability Density Function (PDF) for a set of Power Spectral Densities (PSDs), following *McNamara and Buland* [2004]. We processed time series 2 min long, recorded at both nighttime and daytime with a sampling rate of 62.5 sps; we removed the mean and we applied a digital Butterworth filter with passband $0.05-25$ Hz for the broadband sensors and $0.1-25$ Hz for the short-period ones. Each time series is divided into 8 segments of 40 s, overlapping by 75%, to reduce the variance in the PSD calculation [*Cooley and Tukey*, 1965] and applying a 10% cosine taper to reduce spectral leakage. The spectrum of each segment is computed via the FFTW algorithm [*Frigo and Johnson*, 1998]. Finally, the instrumental response is removed.

[5] The total power, representing the PSD estimate, is obtained from the square of the amplitude spectrum multiplied by the standard normalization factor $2\Delta t/N$, where Δt is the sample interval and N is the number of samples [*McNamara and Buland*, 2004]. The PSD estimate is adjusted for the scale factor (1/0.875) due to cosine tapering [*Bendat and Piersol*, 1971].

[6] The PSD obtained for each 2 minute time series is estimated as the average of the PSDs computed for each of the 8 separate overlapping time segments and converted into decibels with respect to velocity $(m/s)^2/Hz$. Then the PSDs are used to construct the PDF for each station. We compute a distribution of probability at re-sampled discrete frequencies Fc evenly spaced in a logarithmic scale. Each frequency Fc is selected as the geometric mean frequency within a one octave interval, i.e., $Fc = (F_1 * F_2)^{0.5}$, where the considered interval extends from frequency F_1 to $F_2 = 2F_1$. The next Fc is then computed by shifting the interval by one-sixteenth of an octave. Powers

are averaged over ±10% of Fc and grouped into bins 1-dB wide, ranging from −200 to −80 dB. The frequency distribution at each Fc results from the number of spectral estimates that fall into a bin divided the total number of spectral estimates. The PDF has been computed without isolating the horizontal components from the vertical ones. Figure 1 shows the PDFs for the 10 stations described in Table 1. Some stations are equipped with broadband (Nanometrics Trillium, flat response in the frequency range 0.025–50 Hz) or enlarged-band (Lennartz-3D/5s, flat response in the range 0.2–40 Hz range) sensors, while other stations are equipped with short-period sensors (Mark L4-3D or Lennartz-3D Lite/1s). After some calibration tests [see also *Parolai et al.*, 2001], we assume that the power spectra estimated for short-period recordings corrected for instrumental response are reliable for frequencies >0.2 Hz, while the power spectra for broadband or enlarged-band instrumentally corrected recordings will be discussed for frequencies >0.1 Hz. Finally, we also compute the PDF mode, mean, 5th, and 95th percentile.

3. Geological Settings

[7] The investigated area is included in the Alpine orogenesis, a zone between the Africa and Europe convergent plate margins. The post-Oligocene extensional systems in the western Mediterranean, governed by rollback of subduction zones and back-arc extension [*Rosenbaum and Lister*, 2002], concurred to set out the current geomorphological features. In the analyzed area we distinguish two main sectors: the first covers part of the central and Southern Alps, while the second encompasses part of the Po Plain (Figure 1).

[8] The Alpine sector mainly consists of metamorphic basement (hercynian metapelites, minor quartzites, metabasites, marbles, granitoids, orthogneiss) to the north of the Insubric line (Figure 1) and of carbonate platform, basinal and shallow marine deposits (limestones, dolomites, turbidites) in the Southern Alps [*Carminati and Siletto*, 1997; *Milano et al.*, 1988; *Siletto et al.*, 1993]. The Alpine chain is typified by deep valleys filled with glacial and fluvioglacial deposits. The

main valleys led to the Po Plain, with wide morainal amphitheaters.

[9] The Po Plain is a syntectonic sedimentary basin forming the infill of the Pliocene-Pleistocene Apenninic foredeep, bounded by Apennines to the south and by Alps to the north [*Amorosi et al.*, 1996]. The maximum depth of the Quaternary deposits ranges between 1000 and 1500 m [*Pieri and Groppi*, 1981] and covers the foreland of the two mountain chains. The superficial geological layers are fluvial terraces and alluvial deposits. The density of rocks ranges from 2.20 (Quaternary deposits) to 2.80 (Mesozoic rocks) g/cm^3 [*Cassano et al.*, 1986]. On the basis of the shear wave velocity and density values, a heterogeneous distribution of acoustic impedance within the investigated region exists. In particular, a strong lateral contrast between the Alps and the Po Plain is expected, the acoustic impedance being higher in the Alps.

[10] Table 1 shows the main characteristics of the considered seismological stations. The sites are classified by adopting the simplified geological map recently proposed by *Bordoni et al.* [2003]. The outcropping formations are classified into three classes, from rock to soft soil (Table 2), following the EuroCode8 [*European Committee for Standardization*, 2002]. Most of the sites described in Table 1 belong to class A (rock site), even if all the three geological conditions are represented.

4. Infrastructural Settings

[11] The target region (Figure 1) is the most industrialized area of Italy. A significant transport network, with both highways and railways, has been developed in this area where the resident population is about 15 million of inhabitants. Furthermore, the sector of the Po plain included in the investigated area is characterized by an intensive agricultural activity. Thus several strong sources of noise are distributed within this area. A Geographical Information System (GIS) map of the infrastructures has been created to display a likely distribution of the anthropic source of noise (Figure 1). The map shows the density of industries, the most relevant roads and railways, and the

Figure 1. PDFs for the selected sites in north central Italy. The New High Noise Model (black solid line) and the New Low Noise Model (black dashed line) of *Peterson* [1993] are also shown. The map shows the station locations, the infrastructures, the urbanized areas, and the density of industries.
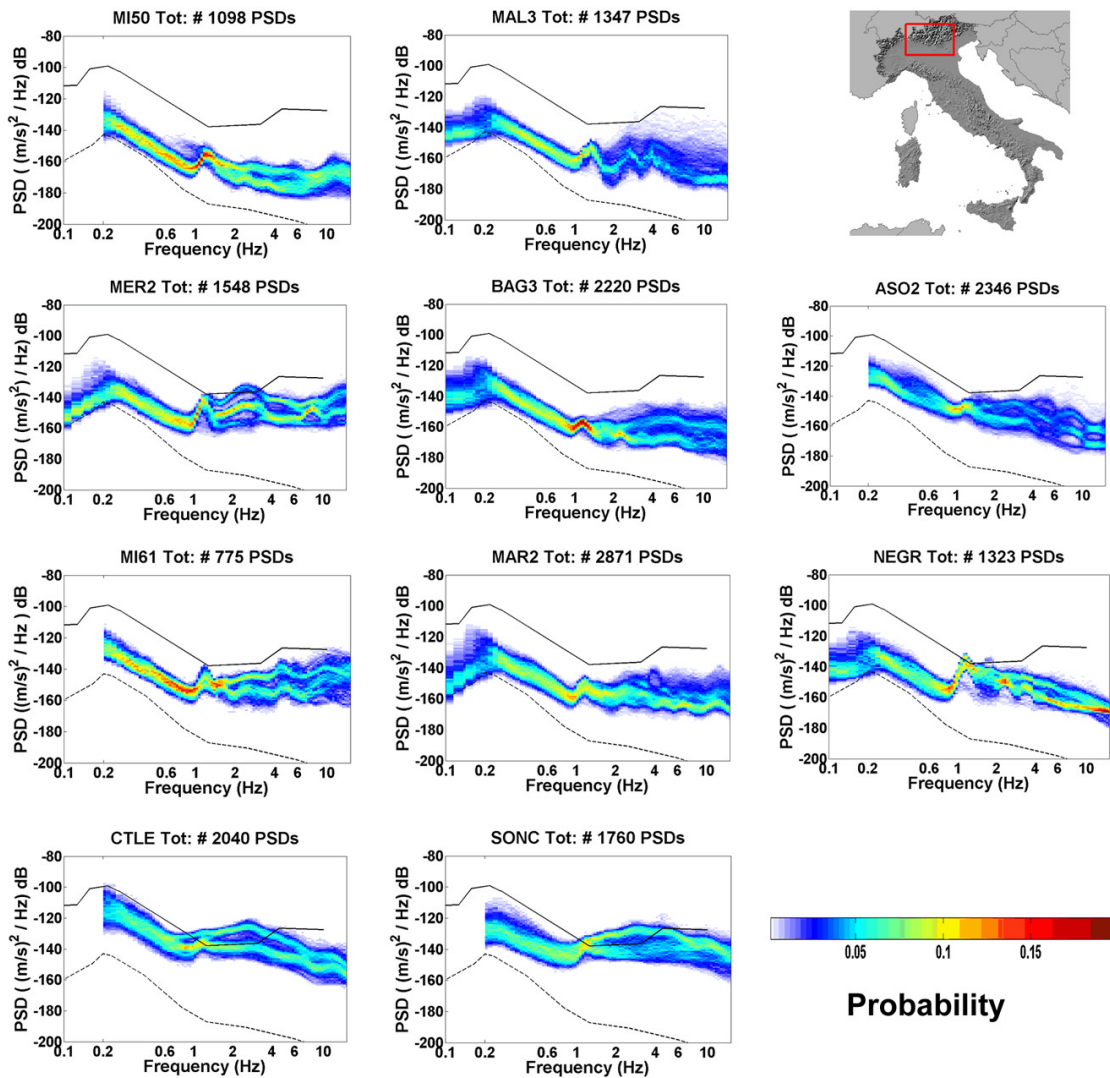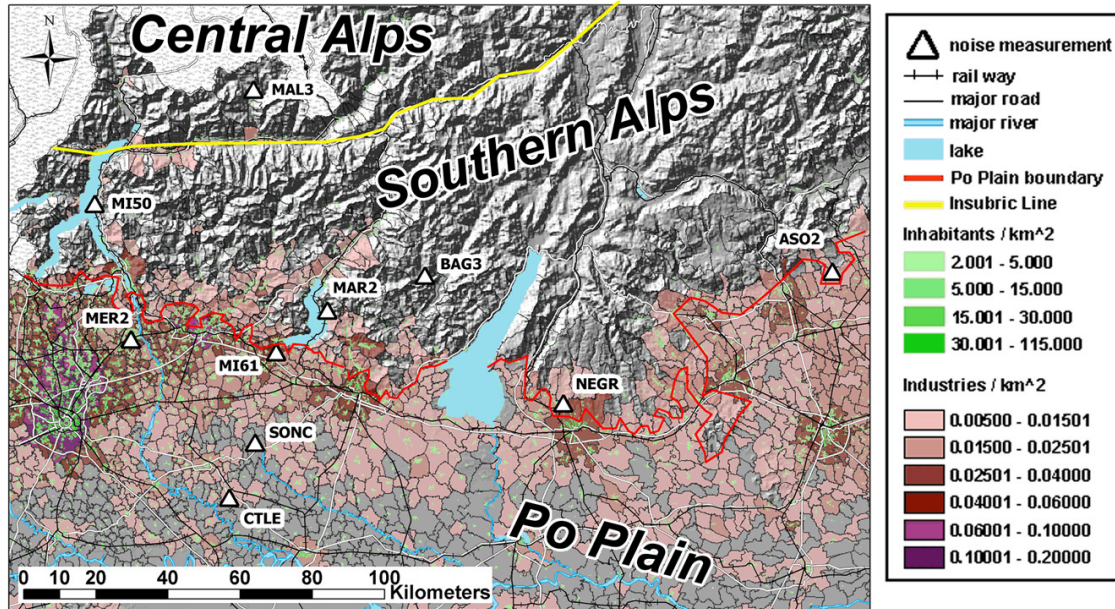
Figure 1

Table 1. Seismological Stations[a]

Code	Long., North	Lat., East	Elevation, m	Sensor	Installation Type	Depth	Class
MI61	9.93	45.64	253	Mark L4 - 3D/1 s	basement of a municipal building	surface	B
MI50	9.29	46.01	219	Mark L4 - 3D/1 s	cave	<10 m	A
SONC	9.86	45.41	90	Mark L4 - 3D/1 s	hole in the ground	surface	B
MAR2	10.12	45.74	600	Nanom. -Trillium/40 s	basement of a little civil building	surface	A
MER2	9.42	45.67	350	Nanom. -Trillium/40 s	concrete in shelter	surface	B
ASO2	11.92	45.8	221	Lennartz - 3D Lite/1 s	medieval fortress on rock	surface	A
NEGR	10.95	45.5	167	Lennartz - 3D/5 s	abandoned iron mine	<10 m	A
BAG3	10.46	45.82	807	Lennartz - 3D/5 s	basement of a school on rock	surface	A
MAL3	9.86	46.29	2030	Lennartz - 3D/5 s	concrete on rock	surface	A
CTLE	9.76	45.27	66	Lennartz - 3D Lite/1 s	basement of a farm	surface	C

[a] The classes are explained in Table 2.

distribution of civil buildings. The density of industries has been computed by normalizing the number of economic entities to the area of the municipal district. The information about the economic entities has been provided by the Italian Institute for Statistics, ISTAT (http://www.istat.it). The informational layer about civil buildings has been derived from the map of census sections as defined in the ISTAT practices. Figure 1 shows that the density of industries, transport ways and civil buildings is higher in the sector between the southern border of the Alps and the northern part of the Po Plain.

5. Discussion

[12] The background seismic noise is generated by several types of sources. While the high frequency seismic noise (frequency >1 Hz) is mainly caused by man-made activities [*Kulhanek*, 1990; *Okada*, 2003; *McNamara and Buland*, 2004], the seismic noise for frequency <1 Hz is mainly determined by

weather conditions [e.g., *Longuet-Higgins*, 1950; *Friedrich et al.*, 1998]. In this section, we detail the noise power estimated for the selected sites considering the frequency bands 0.1–1 Hz and 1–15 Hz separately.

5.1. Frequencies >1 Hz

[13] Man-made activities are the dominant sources of high-frequency noise, referred to as cultural noise and originated from the coupling of traffic and machinery energy into the Earth. Figure 1 shows the PDFs for the analyzed stations. Since the cultural noise attenuates within several kilometers in distance, both the level and the shape of the noise power in the high-frequency range are strongly different from site to site. The highest noise levels are observed for those stations located close to areas with high density of industries and infrastructures (MER2, MI61, SONC, CTLE, NEGR, ASO2). In particular, the PDFs for stations CTLE and SONC, located in the middle of the Po Plain, exceed the New High Noise Model (NHNM)

Table 2. Geological Description of the Considered Sites[a]

Class	Lithotype	Vs, m/s	Description
A	rock	>800	Marine clay and all the others rocks (Lower Pleistocene and Pliocene); volcanic rock and deposits
B	stiff soil	400 < Vs < 800	colluvial, alluvial, lacustrine, beach, fluvial terraces, glacial deposits and clay (Middle-Upper Pleistocene); sand and loose conglomerate (Pleistocene and Pliocene); travertine (Pleistocene and Holocene)
C	soft soil	<400	colluvial, alluvial, lacustrine, beach, fluvial terraces deposits (Holocene)

[a] The lithotypes are grouped into three categories, A, B, and C, following *Bordoni et al.* [2003].
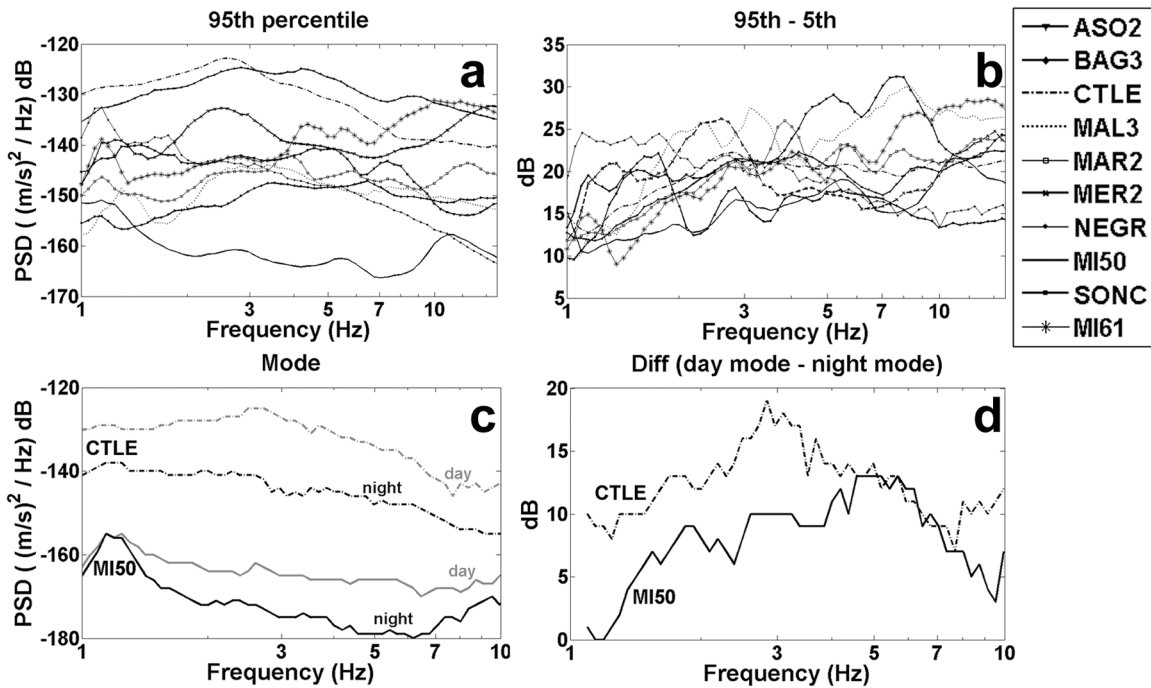
Figure 2. (a) PDF 95th percentile for the considered seismic stations. (b) Difference between the 95th and 5th percentile of PDF for each station. (c) PDF mode for stations CTLE (dash-dotted line) and MI50 (solid line), considering diurnal (gray) and night (black) recordings. (d) Difference between day and night modes for CTLE (dash-dotted line) and MI50 (solid line).

of *Peterson* [1993] for frequencies in the range 1–5 Hz. Lower noise levels are observed for stations installed in the Alpine environment, such as station MI50, which is installed in a cave few meters below the surface, and stations MAR2 and BAG3, which are located in an isolated site and in a little village, respectively. Station MAL3 is installed in the central Alps, at an altitude of 2030 m. It shows a low background noise level but the presence of a skiing area, with lifts and cableways, introduces some disturbances at frequencies >2 Hz. Moreover, the noise levels for station MAL3 are also affected by the activity of the mining industries deployed in the valleys below the recording site. The variability of the background noise level in north central Italy is summarized in Figure 2a, where the 95th percentiles of the PDFs for different sites are compared. The values assumed by this percentile vary from −165 to −125 dB (relative to $(m/s)^2$/Hz). Figure 2b shows the differences between the 95th and the 5th percentiles. The differences, and hence the dispersion of the powers, show a positive trend with frequency for all sites. The differences are lower than 20 dB at 1 Hz but they exceed 25 dB for frequencies >2 Hz. The variability results from the diurnal variation of the noise levels, as shown in Figure 2c. This panel exemplifies the

diurnal variation for stations MI50 (a quiet site on rock) and CTLE (a noisy site on sediments). The power spectral densities of records acquired at 1300 UTC and 0200 UTC are considered to evaluate the day and night PDFs, respectively. The trends of the day and night PDF modes are similar but the day level is from 10 to 20 dB higher than the night level at CTLE, and up to 10 dB higher at MI50, as shown in Figure 2d. Diurnal variations can be observed for most of the considered stations. Figure 1 shows that the PDFs for sites exposed to strong cultural noise are generally bi-modal, each branch being representative of the noise power during either the day or night hours.

[14] The difference of 40 dB among the noise powers shown in Figure 2a could affect the detection threshold of local earthquakes in the analyzed region. A noise reduction of about 20 dB for CTLE could be achieved by installing a borehole sensor [*Cocco et al.*, 2001]. The influence of the noise levels on the detection threshold is exemplified in Figure 3. In this figure, the spatial variability of the magnitude corresponding to the detection threshold (hereinafter referred to as magnitude threshold) is estimated by comparing the average noise levels at each station with a synthetic spectrum. The syn-
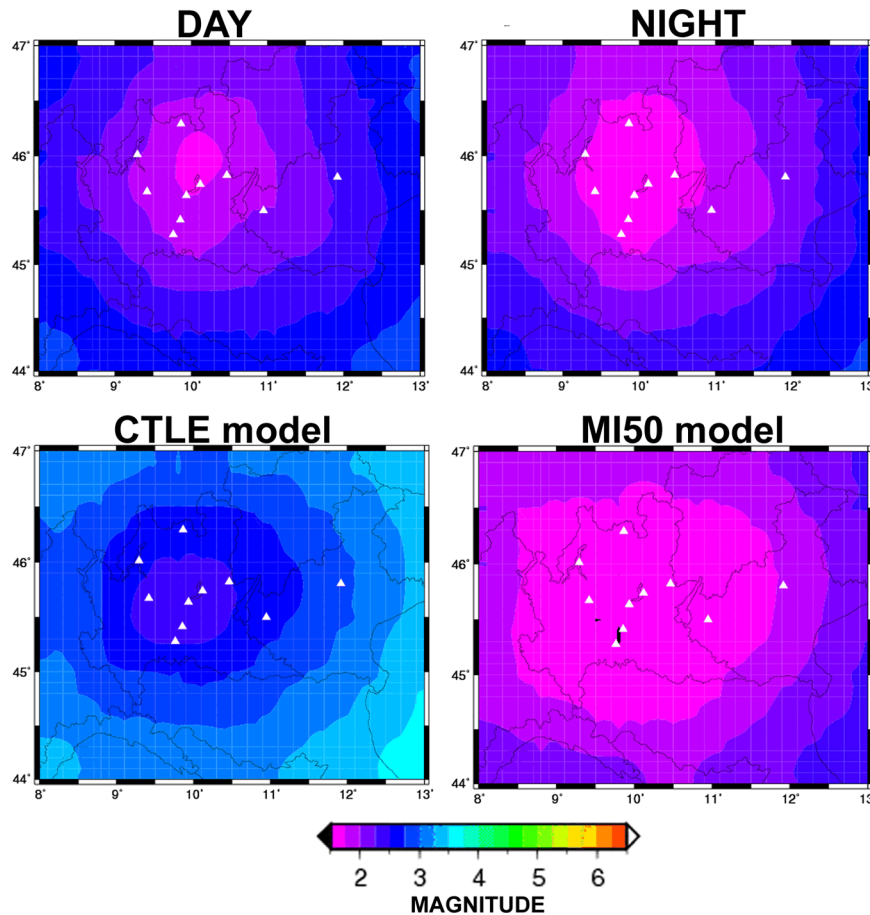
Figure 3. Results of the synthetic test performed for estimating the spatial variability of the detection thresholds of the network deployed in the analyzed area (white triangles). Top panels: the threshold magnitude has been computed by comparing the average daytime (left panel) and nighttime (right panel) noise levels at each station with the *Brune* [1970] source model attenuated for the 1/R geometrical spreading. Bottom panels: detection thresholds estimated using the daytime average noise level of station CTLE (left panel) and the nighttime average noise level of station MI50 (right panel) for all the stations.

thetic spectrum is computed by considering the ω-square source model [*Brune*, 1970] for a distribution of earthquakes located at each node of a regular grid having a step of 25 km. The source spectrum is propagated to each station considering the 1/R geometrical spreading term. We assumed that an earthquake is detected by the network when the signal-to-noise ratio, computed over the 1 to 10 Hz frequency range, is larger than 3 for three stations, at least. During the day hours (top left panel), the smallest magnitude thresholds are relevant to earthquakes occurring within the area delimited by the stations installed in the Alpine environment, while during the nighttime (top right panel) the area corresponding to the smallest detection thresholds becomes wider since the noise levels at the stations installed in the Po Plain decrease during the nighttime. To stress the influ-

ence of the noise levels on the detection threshold, the bottom frames of Figure 3 show the estimated magnitude thresholds assuming that all the stations have a noise level equals to either the noise level at station CTLE during the daytime (bottom left panel), or the level estimated for station MI50 during the nighttime (bottom right panel). While in the former case the smallest detected threshold is close to 2.5, in the latter case the threshold magnitude is <2 for earthquakes occurring within a wide area.

[15] Figure 1 shows that a peak around 1.1 Hz is present in the PDFs for the considered sites, event if it is partially masked by the high level of the background noise affecting the recordings of some stations (e.g., SONC and CTLE). Figure 4, top panel, exemplifies the variation with time of the PSD maximum in the range 1–1.2 Hz, considering
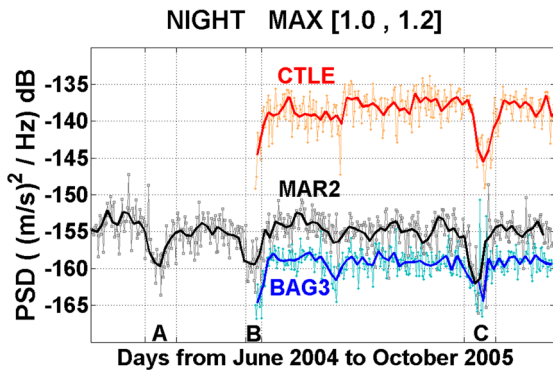
Figure 4. Night PSD maximum values in the range 1.0–1.2 Hz for stations CTLE, MAR2, and BAG3 from June 2004 to October 2005. The solid lines are the moving averages computed over five measurements. Sectors A and C identify August 2004 and 2005, respectively. Sector B ranges from 23 December 2004 to 9 January 2005.

the night recordings at stations BAG3, MAR2, and CTLE. The maxima oscillate around an average value of −159 dB, −155 dB, and −137 dB for BAG3, MAR2 and CTLE stations, respectively, excluding three intervals where a significant diminishment of the maxima takes place. The intervals A and C correspond to August 2004 and 2005, respectively, whereas interval B spans the days from 23 December 2004 to 9 January 2005. Since the three intervals correspond to periods of low industrial and anthropic activities (summer and Christmas holidays in Italy), we conclude that the 1.1 Hz peak is correlated with the level of the anthropic activities. Array measurements will be performed both to determine the noise sources for the 1.1 Hz peak and to investigate alternative explanations for its origin [e.g., *Correig and Urquizú*, 2002], since the presence of a spectral

peak at multiple stations with a constant frequency could be exploited to study temporal variation in the properties of the Earth's crust.

5.2. Frequencies in the Range 0.1–1 Hz

[16] In the frequency range 0.1–1 Hz, the PDFs shown in Figure 1 are dominated by a peak called the double-frequency (DF) peak [*Longuet-Higgins*, 1950]. It is generated by ocean waves traveling in opposite directions and having equal period; the superposition of these waves generates gravity standing waves of half-period that cause a non-linear pressure perturbation that propagates to the ocean bottom. The DF microseism level depends on the amplitude of ocean waves, the size of the generation region and on the propagation characteristics [*Longuet-Higgins*, 1950; *Hasselmann*, 1963; *Friedrich et al.*, 1998; *Bromirski and Duennebier*, 2002]. The correlation between the DF peak and the presence of ocean storms is supported by the observation of seasonal variability of the DF features. Figure 5 shows the noise seasonal variability for station MAR2, which is equipped with a broadband sensor. We estimated the PDF by considering the summer (left panel) and winter (middle panel) recordings. For frequencies <1 Hz, the seasonal variability of noise is evident. In winter, the noise power is higher than in summer and the peak of the mode is shifted toward lower frequencies (Figure 5, right panel), in agreement with earlier works [e.g., *Stutzmann et al.*, 2000]. It is worth noting that the winter and summer noise levels shown in Figure 5 are similar for frequencies >1 Hz since the short-period background noise is mainly dominated by man-made activities, as previously discussed. Figure 6 shows the maximum values, in the range 0.1–0.3 Hz, of the power spectral densities relative to 2872 daily recordings
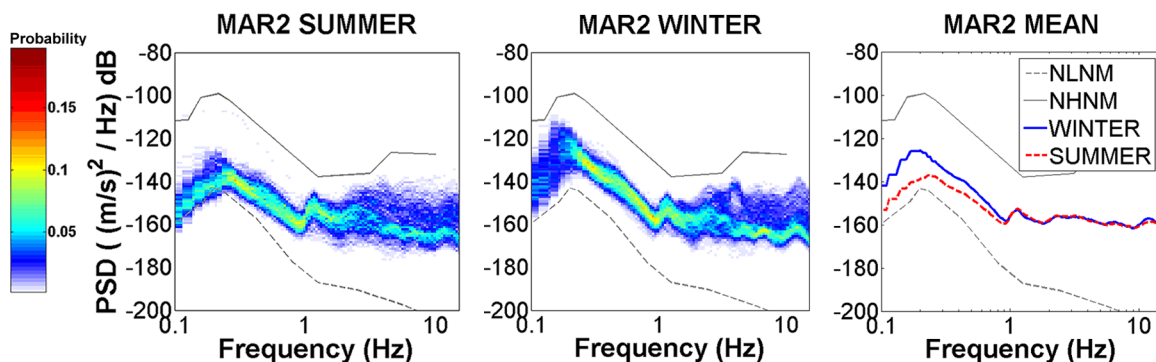

Figure 5. Seasonal variations of noise level for station MAR2. (left) PDF of summer recordings; (middle) PDF of winter recordings; and (right) PDF mode of winter (blue solid line) and summer (red dashed line) recordings.
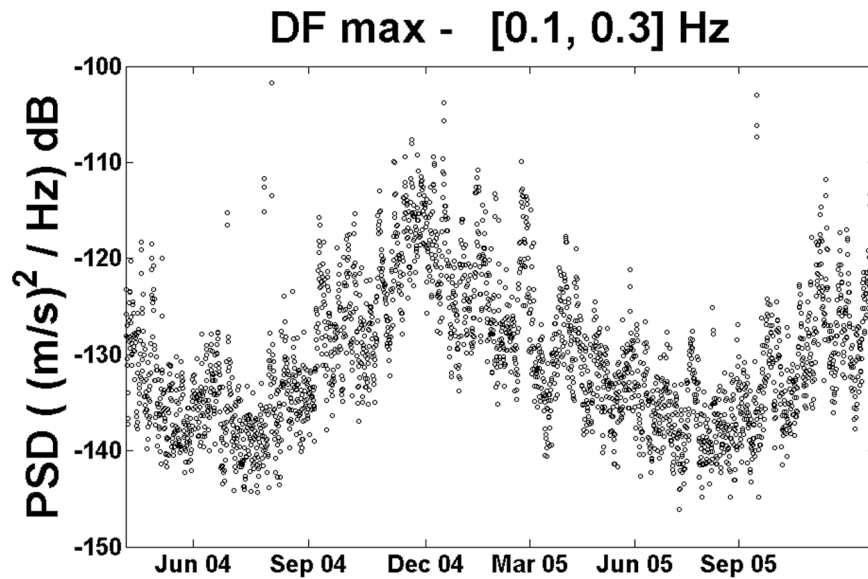
Figure 6. Maximum values of PSD in the range $0.1-0.3$ Hz for station MAR2. Recordings at 0200 UTC and 1200 UTC from March 2004 to November 2005 are considered.

from March 2004 to November 2005. The correlation of DF level with seasons is evident for station MAR2 and the maximum values show a periodic behavior with a difference of about 25 dB between the winter and summer recordings. Some values behave as outliers with respect to the mean trend. Most of these values are relative to the DF microseisms generated by intense Atlantic storms. Figure 7 shows the example of September 2005. We detect some significant meteorological events by analyzing the barometric maps of Atlantic Ocean and Europe collected from the UK Meteorological Office (http://www.metoffice.gov.uk/weather/charts/index.html) and the sea height measured at two buoys belonging to the Rete Ondametrica Italiana (http://www.apat.gov.it). During the days 14, 21, and 27 September, three strong DF peaks appear in spectral components of station MAR2, in the range $0.10-0.25$ Hz; in correspondence to these days, deep sea level pressure minima are present over the North Atlantic Ocean (Figure 7). The locations of the barometric minima suggest the presence of North Atlantic storms able to generate the DF microseisms within some of the source regions previously detected by *Friedrich et al.* [1998]. They analyzed broadband continuous recordings at the Gräfenberg array (southern Germany, about 500 km north of the Po Plain) to locate the generating areas of DF microseisms. Performing a frequency-wave number analysis, they identified five source areas: the strongest source is located near the north Norwegian coast

while minor sources are located in the Atlantic Ocean at the latitudes of Ireland and France (for details, see Figure 6 of *Friedrich et al.* [1998]). Finally, they detected a source region also in the Mediterranean Sea. The locations of the strongest events in Figure 7, which occurred on 21 and 27 September, are in good agreement with two of the source regions identified by *Friedrich et al.* [1998].

[17] The PSDs in Figure 7 show the presence of DF peaks also in the range $0.25-0.50$ Hz. The presence of two frequency bands for the DF peak is emphasized in the left middle panel of Figure 7, where the PSD is normalized to the mean spectral amplitude at each frequency [*Bromirski et al.*, 2005]. Figure 8 shows the height of the sea waves measured at two buoys deployed in the Tyrrhenian Sea (buoy LSP) and in the Adriatic Sea (buoy ANC). The frequency and azimuth of sea waves measured at the buoys on 12, 17, 18, and 29 September are also shown. The frequency ranges from 0.15 to 0.22 Hz and the propagation azimuths are about $63°$ and $220°$ for the Adriatic and Tyrrhenian seas, respectively, which means that the sea waves propagate almost perpendicular to the coasts. If we assume that a superposition of these waves and those reflected from the shorelines are able to generate gravity standing waves of half-period, then the observed maxima in the range $0.25-0.50$ Hz are quite well correlated to the local conditions in the Adriatic and Tyrrhenian seas. The splitting of the DF peak into two peaks has been
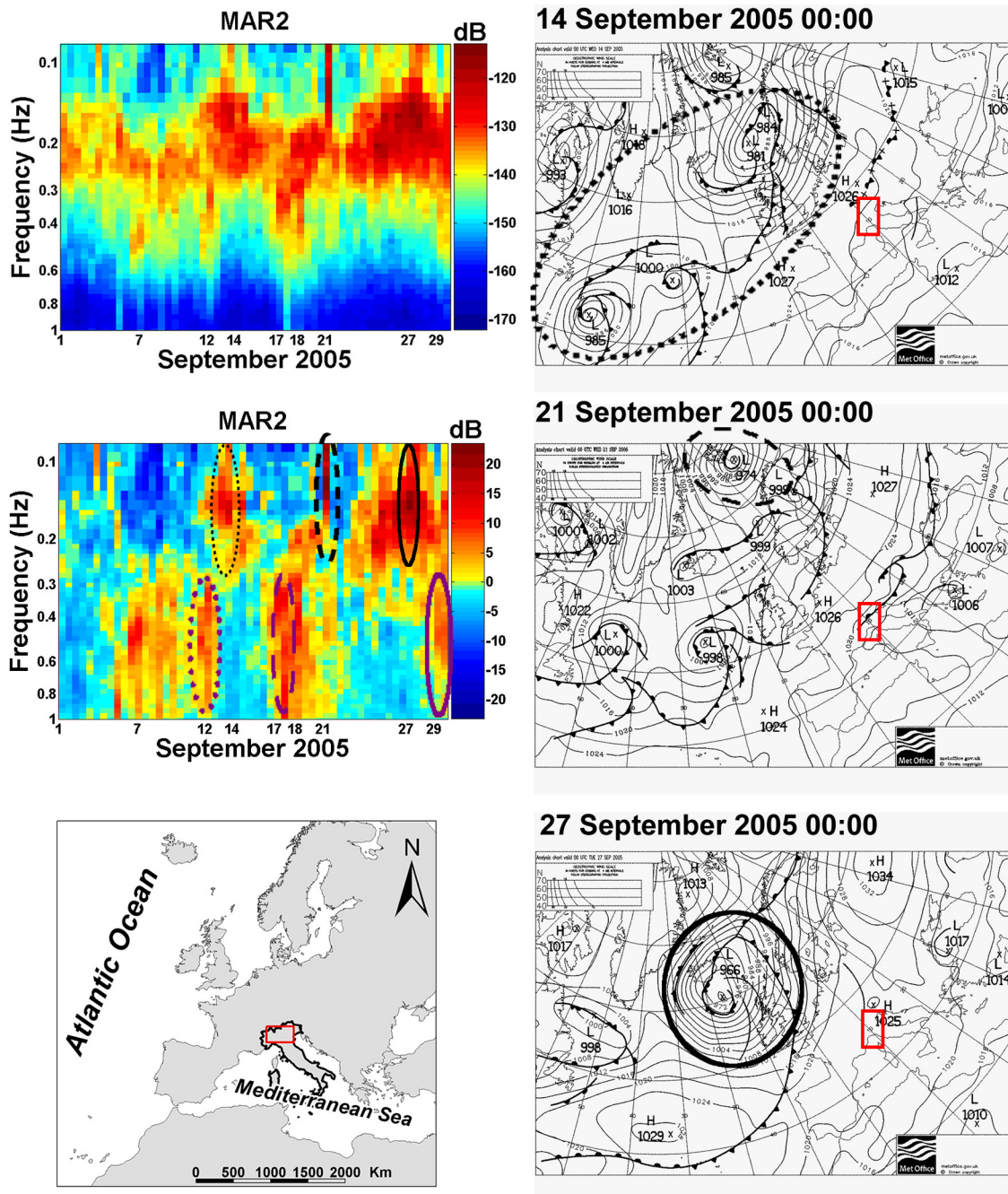
Figure 7. (top left) PSDs in the frequency band 0.1–1.0 Hz, for station MAR2 during September 2005. (middle left) The same as in the top left panel but the PSDs are normalized to the mean spectral amplitude at each frequency. The right panels show, from top to bottom, the barometric maps of 14, 21, and 27 September 2005. The black ellipses highlight the barometric minima over the Atlantic Ocean and the respective associated values of PSD for station MAR2. The red rectangles delimit the investigated area in north central Italy (bottom left). The purple ellipses refer to Figure 8. The maps have been provided by the UK Meteorological Office (http://www.metoffice.gov.uk/weather/charts/index.html).

previously observed by *Stephen et al.* [2003] and *Bromirski et al.* [2005]. In particular, *Bromirski et al.* [2005], who referred to these peaks as long-period DF (LPDF) and short-period DF (SPDF),

concluded that short-period DF microseisms are generated by rapid shift of local winds and by nearby storms [see also *Kibblewhite and Ewans*, 1985; *Herbers and Guza*, 1994] while long-period
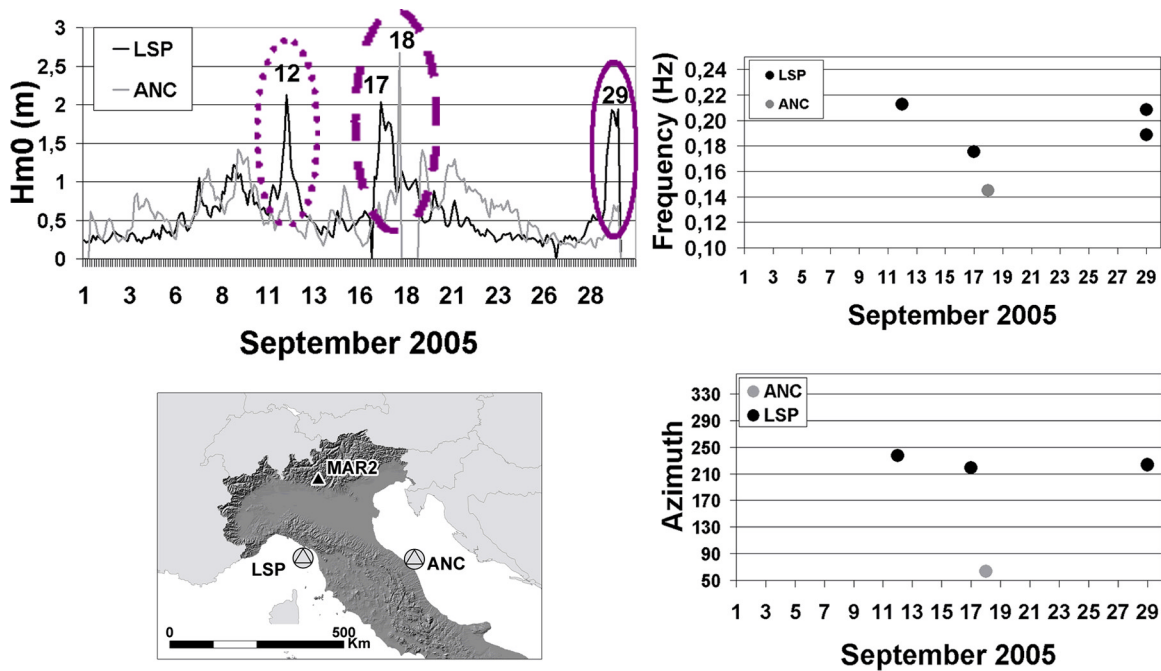
Figure 8. Data relative to buoys located in the Tyrrhenian Sea (LSP) and in the Adriatic Sea (ANC) operated by the Rete Ondametrica Nazionale. (bottom left) Locations of the buoys (LSP, ANC) and the seismic station (MAR2). (top left) Average height (Hm0) of sea wave at LSP (black) and ANC (gray) during September 2005; the purple ellipses highlight the maximum amplitude of waves, and the respective associated values of the PSD are shown in Figure 7. Both the recorded sea wave frequency (top right) and azimuth (bottom right) relevant to the maximum sea height during 12, 17, 18, and 29 September 2005 are also shown.

DF microseisms are often generated in near-coastal areas, where the swells from distant storms are reflected by the shoreline, and only under favorable weather conditions in the open ocean [see also *Bromirski and Duennebier*, 2002]. Furthermore, *Bromirski et al.* [2005] showed that the energy associated to the SPDF does not propagate efficiently along the oceanic floor and it attenuates within few hundred kilometers. In our case, the LPDF microseisms are generated in the North Atlantic Ocean and travel for some thousand kilometers through the European continental crust, while the SPDF microseisms seems to be generated in the Mediterranean Sea, few hundred kilometers far from the considered sites.

5.3. Noise Reduction due to Lateral Impedance Contrast

[18] Finally, we investigate the reduction of noise power when the seismic waves propagate across two adjacent media with different acoustic impedance, defined as the product between the seismic velocity and density of each medium. Figure 9 shows the PDFs for three stations installed in different geological contexts: station MAR2 is installed on rocks in the southern Alps (class A of Table 1), station CTLE is installed over a thick sedimentary cover in the Po plain (class C) and ASO2 site is located on a Pliocene hill at the margin of the Po Plain, partially covered by Po Plain sediments (class B). Since the power spectra for frequency >1 Hz are strongly influenced by the man-made activities and the maximum amplitude of the DF peak cannot be reliably estimated because CTLE and ASO2 are equipped with short-period sensors, we compare the 5th percentile of PDFs over the frequency range 0.2–0.6 Hz. We observe an average power reduction for MAR2 of about 15 dB and 7 dB when compared with the powers for CTLE and ASO2, respectively. The stronger reduction of noise power between CTLE and MAR2 agrees with a higher average lateral impedance contrast between the Po Plain and the Alps than the average impedance contrast between the Pliocene hills and the Alps. To confirm the role played by the geology in the reduction of noise power, Figure 10 compares the power spectral density computed at stations CTLE and MAR2 for data recorded on 17 September 2005 (at 0230 UTC) and on 27 September 2005 (at 0230 UTC), that we previously discussed (Figures 7 and 8). In
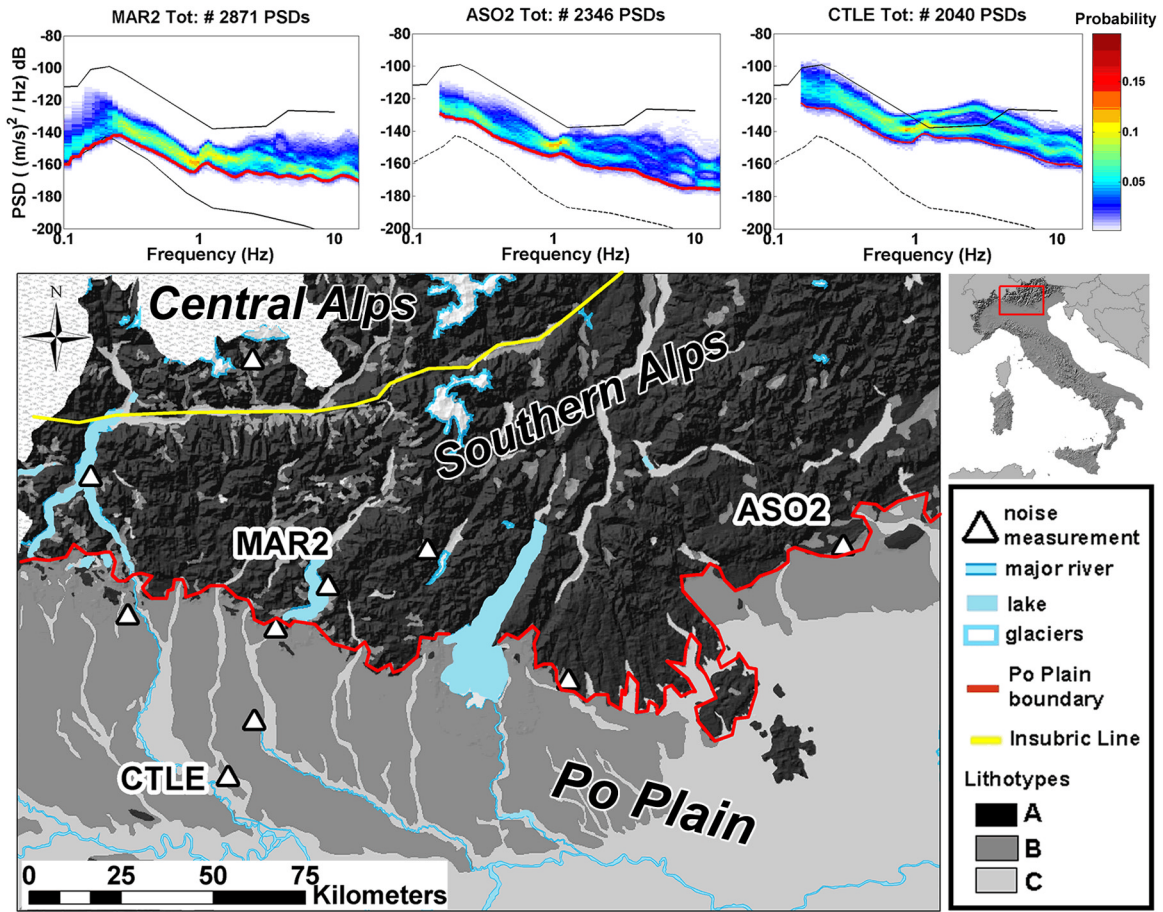
Figure 9. PDFs for stations MAR2, ASO2, and CTLE. Red lines in top panels are the 5th percentiles of PDFs. The map shows the different lithotypes (Table 2) and the location of seismic stations.

the former case, microseisms generated in the Tyrrhenian Sea propagate from south to north, while in the latter case microseisms generated in the North Atlantic Ocean propagate in the opposite direction. In the frequency range 0.2–0.6 Hz, the average reduction of noise power from CTLE to MAR2 is about 10 dB. The observed reduction can be used to estimate, at least roughly, the average impedance contrast between the Po Plain and the Alps [*Bormann et al.*, 1997]. In the case of vertical incidence of the wavefront from a medium 1 to a medium 2, the amplitude ratio of the transmitted wave as compared to the incident wave is [e.g., *Lay and Wallace*, 1995]

$$\frac{A_2}{A_1} = 2\frac{V_1\rho_1}{V_1\rho_1 + V_2\rho_2} \qquad (1)$$

where V_1 and ρ_1 are the velocity and density of medium 1 and V_2, ρ_2 those of medium 2. If we

simplify the geological setting of the analyzed region considering only two homogeneous media with a sharp lateral impedance contrast between them, then we can apply (1) locating CTLE in medium 1 and MAR2 in medium 2. The difference of 10 dB between the noise powers corresponds to about a factor 5 between the impedance of the two media ($V_2\rho_2 \sim 5.3V_1\rho_1$).

6. Conclusions

[19] The characteristics of background seismic noise in north central Italy have been investigated by means of velocity power spectral analysis [*McNamara and Buland*, 2004], within the frequency range 0.1–15 Hz. The noise powers exhibit considerable variations in the range 1–15 Hz, since the noise recordings are strongly affected by man-made activities. The observed differences of 40 dB among the 95th percentile of the probability den-
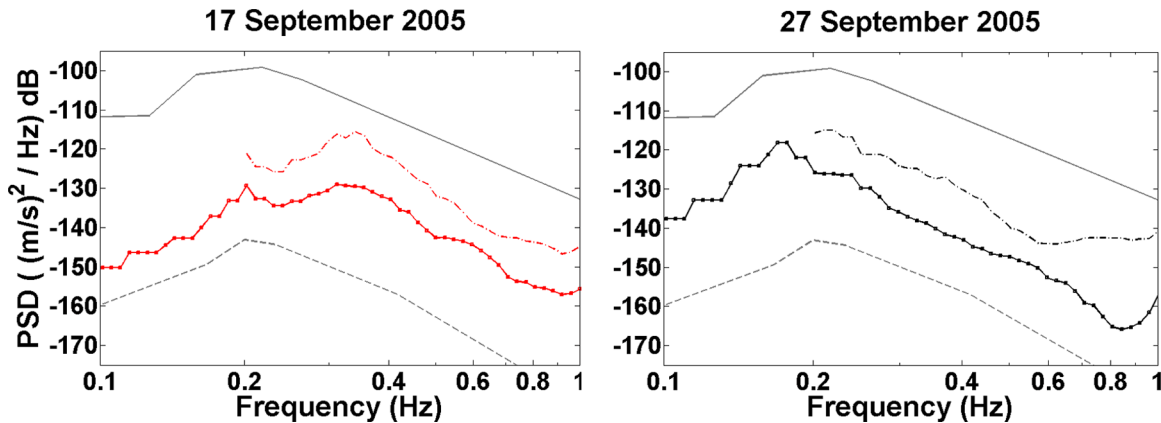
Figure 10. (left) PSD for stations CTLE (dash-dotted line) and MAR2 (solid line) during 17 September 2005 at 0230 UTC. (right) PSD for station CTLE (dash-dotted line) and station MAR2 (solid line) during 27 September 2005 at 0230 UTC.

sity functions for different stations has to be considered in the design of a network for recording the small to moderate size seismicity occurring in north central Italy. In particular, the high noise level characterizing the site in the Po Plain and in the sector between the Po Plain and the Southern Alps could limit the detection of weak earthquake motions. We observed that the double frequency microseism band is divided into two bands, depending on the location of the source of microseisms. The DF peak is in the range 0.10–0.25 Hz for microseisms generated in the North Atlantic Ocean while it moves toward frequencies higher than 0.25 Hz when the microseisms are locally generated in the Mediterranean Sea. Finally, the reduction of noise power in the microseism frequency band, due to the seismic impedance contrast between the Po Plain and the Alps, has been estimated. Future work will be devoted to performing array measurements to detect the locations of the microseism sources. Moreover, continuous recordings from broadband stations will be acquired to characterize in more detail the propagation characteristics of the microseisms in north Italy and to detect the microseisms generated in the large lakes present in this area.

Acknowledgments

References

Amorosi, A., M. Farina, P. Severi, D. Preti, L. Caporale, and G. Di Dio (1996), Genetically related alluvial deposits across active fault zones: An example of alluvial fan-terrace correlation from the upper Quaternary of the southern Po Basin, Italy, *Sediment. Geol.*, *102*, 274–295.

Bendat, J. S., and A. G. Piersol (1971), *Random Data: Analysis and Measurement Procedures*, 407 pp., Wiley-Interscience, Hoboken, N. J.

Bordoni, P., F. Marra, M. Moro, L. Luzi, and L. Margheriti (2003), Geological class map, in *Terremoti Probabili in Italia tra l'Anno 2000 e il 2030: Elementi per la Definizione di Priorità Degli Interventi di Riduzione del Rischio Sismico*, Annex 1, Task 3.2, pp. 3–4, GNDT Proj., Rome.

Bormann, P. (2002), Seismic signals and noise, in *IASPEI New Manual of Seismological Observatory Practice*, vol. 1, edited by P. Bormann, chap. 4, pp. 1–33, GeoForschungs-Zentrum, Potsdam, Germany.

Bormann, P., K. Wylegalla, and K. Klinge (1997), Analysis of broadband seismic noise at the German Regional Seismic Network and search for improved alternative station sites, *J. Seismol.*, *1*, 357–381.

Bromirski, P. D., and F. K. Duennebier (2002), The near-coastal microseism spectrum: Spatial and temporal wave climate relationships, *J. Geophys. Res.*, *107*(B8), 2166, doi:10.1029/2001JB000265.

Bromirski, P. D., F. K. Duennebier, and R. A. Stephen (2005), Mid-ocean microseisms, *Geochem. Geophys. Geosyst.*, *6*, Q04009, doi:10.1029/2004GC000768.

Brune, J. N. (1970), Tectonic stress and the spectra of seismic shear waves from earthquakes, *J. Geophys. Res.*, *75*, 4997–5009.

Carminati, E., and G. B. Siletto (1997), The effects of brittle-plastic transitions in basement-involved foreland belts: The Central Southern Alps case (N Italy), *Tectonophysics*, *280*, 107–123.

Cassano, E., L. Anelli, R. Fichera, and V. Cappelli (1986), Pianura Padana—Interpretazione integrata di dati geofisici e geologici, paper presented at 73rd Congresso Società Geologica Italiana, Roma, 29 Sept. to 4 Oct.

Cocco, M., F. Ardizzoni, R. M. Azzara, L. Dall'Olio, A. Delladio, M. Di Bona, L. Malagnini, L. Margheriti,

and A. Nardi (2001), Broadband waveforms and site effects at a borehole seismometer in the Po alluvial basin (Italy), *Ann. Geofis.*, *44*(1), 137–154.

Cooley, J. W., and J. W. Tukey (1965), An algorithm for machine calculation of complex Fourier series, *Math. Comput.*, *19*, 297–301.

Correig, A. M., and M. Urquizú (2002), Some dynamical characteristics of microseism time-series, *Geophys. J. Int.*, *149*, 589–598.

European Committee for Standardization (2002), Design provisions for earthquake resistance of structures: Seismic actions and general requirements of structures (draft), *CEN/TC 250, ENV 1998-1-1, EUROCODE 8*, Brussels, May.

Friedrich, A., F. Krüger, and K. Klinge (1998), Ocean generated microseismic noise located with the Gräfenberg array, *J. Seismol.*, *2*, 47–64.

Frigo, M., and S. G. Johnson (1998), FFTW: An adaptive software architecture for the FFT, in *Proceedings of the 1998 IEEE International Conference on Acoustics, Speech And Signal Processing*, vol. 3, pp. 1381–1384, Int. Electron. and Electr. Eng., New York.

Hasselmann, K. (1963), A statistical analysis of the generation of microseisms, *Rev. Geophys.*, *1*, 177–210.

Herbers, T. H. C., and R. T. Guza (1994), Wind-wave nonlinearity observed at the seafloor, Part I: Forced-wave energy, *J. Phys. Oceanogr.*, *21*(12), 1740–1761.

Kibblewhite, A. C., and K. C. Ewans (1985), Wave-wave interactions, microseisms, and infrasonic ambient noise in the ocean, *J. Acoust. Soc. Am.*, *78*, 981–994.

Kulhanek, O. (1990), *Anatomy of Seismograms: Development in Solid Earth Geophysics*, 178 pp., Elsevier, New York.

Lay, T., and T. C. Wallace (1995), *Modern Global Seismology*, 521 pp., Elsevier, New York.

Longuet-Higgins, M. S. (1950), A theory of the origin of microseisms, *Philos. Trans. R. Soc. London, Ser. A*, *243*, 2–36.

Milano, P. F., G. Pennacchioni, and M. I. Spalla (1988), Alpine and pre-Alpine tectonics in the Central Orobic Alps (Southern Alps), *Eclogae Geol. Helv.*, *81*, 273–293.

McNamara, D. E., and R. P. Buland (2004), Ambient noise levels in the continental United States, *Bull. Seismol. Soc. Am.*, *94*(4), 1517–1527.

Okada, H. (2003), *The Microtremor Survey Method*, *Geophys. Monogr. Ser.*, vol. 12, edited by D. V. Fitterman, and M. W. Asten, 135 pp., Soc. of Explor. Geophys., Tulsa, Okla.

Parolai, S., P. Bormann, and C. Milkereit (2001), Assessment of the natural frequency of the sedimentary cover in the Cologne area (Germany) using noise measurements, *J. Earthquake Eng.*, *5*(4), 541–564.

Peterson, J. (1993), Observations and modeling of background seismic noise, *U.S. Geol. Surv. Open File Rep., 93-322*.

Pieri, M., and G. Groppi (1981), Subsurface geological structure of the Po Plain, in *Progetto Finalizzato Geodinamica*, pp. 1–11, Cons. Naz. delle Ric., Rome.

Rosenbaum, G., and G. S. Lister (2002), Reconstruction of the evolution of the Alpine-Himalayan orogen—An introduction, *J. Virtual Explor.*, *8*, 1–2.

Siletto, G. B., M. I. Spalla, A. Tunesi, J. M. Lardeaux, and A. Colombo (1993), Pre-Alpine structural and metamorphic histories in the Orobic Southern Alps, Italy, in *Pre-Mesozoic Geology in the Alps*, edited by J. F. Von Raumer and F. Neubauer, pp. 585–598, Springer, New York.

Stephen, R. A., F. N. Spiess, J. A. Collins, J. A. Hildebrand, J. A. Orcutt, K. R. Peal, F. L. Vernon, and F. B. Wooding (2003), Ocean Seismic Network Pilot Experiment, *Geochem. Geophys. Geosyst.*, *4*(10), 1092, doi:10.1029/2002GC000485.

Stutzmann, E., G. Roult, and L. Astiz (2000), GEOSCOPE station noise levels, *Bull. Seismol. Soc. Am.*, *90*(3), 690–701.

Trnkoczy, A., P. Bormann, W. Hanka, L. G. Holcomb, and R. L. Nigbor (2002), Site selection, preparation and installation of seismic station, in *IASPEI New Manual of Seismological Observatory Practice*, vol. 1, edited by P. Bormann, chap. 7, pp. 1–106, GeoForschungsZentrum, Potsdam.